2021-12-30

Study of fluidstructure interaction with undulating flow using channel driven cavity flow system

Klein, N.; Kwon, Y.W.; Didoszak, J.M.; Burns, E.; Sachau, D.

Springer

Klein, N., et al. "Study of fluidstructure interaction with undulating flow using channel driven cavity flow system." Multiscale and Multidisciplinary Modeling, Experiments and Design 5.2 (2022): 199-213.
http://hdl.handle.net/10945/71305

Multiscale and Multidisciplinary Modeling, Experiments and Design (2022) 5:199–213
https://doi.org/10.1007/s41939-021-00112-7

ORIGINAL PAPER

Study of fluid–structure interaction with undulating flow using channel driven cavity flow system

N. Klein[1,2] · Y. W. Kwon[1] · J. M. Didoszak[1] · E. Burns[3] · D. Sachau[2]

Received: 26 October 2021 / Accepted: 15 December 2021 / Published online: 30 December 2021

Abstract
Fluid–structure interaction (FSI) induced by undulated flows was investigated using a channel driven cavity flow (CDCF) system. The bottom of the cavity section has a flexible plate made of either an aluminum alloy or carbon fiber composite, which interacts with flows in the cavity. Undulating flows were generated by controlling a series of solenoid valves programmed to interrupt the flow at various different frequencies from 0.5 to 1.25 Hz. Mean flow velocity was also varied for each given undulation frequency. The dynamic motion of the flexible test panel, made of aluminum alloy or carbon fiber composite, was measured for transverse deflections using laser displacement sensors. The study showed that the structural response was very dependent on the input flow. The plate vibrational modes had three to five dominant frequencies ranging from the undulated flow frequencies to about 5.0 Hz. Those frequencies were either at or very close to the multiples of the flow frequencies. The most dominant frequency was not always the same as the flow frequency, but it varied depending on the applied flow frequency.

Keywords Fluid–structure interaction · Channel driven cavity flow · Undulated flow · Composite

1 Introduction

Fluid–structure interaction (FSI) is one of the most common multiphysics problems in engineering. Fluid–structure interaction generally describes the synergy between a flexible structure and a moving fluid. In other words, FSI describes how an external or internal fluid flow (e.g., water, air, etc.) affects a deformable structure or vice versa.

One of the typical FSI problems is the flow-induced vibrations (FIV). There has been extensive research on this topic (Blake 2017a, b; Blevins 1977, 1979; Nakamura et al. 2013; Naudascher and Rockwell 1994; Pettigrew et al. 1998; Leonard and Roshko 2001; Chen 1968). One set of FIV cases is that of externally induced excitation resulting from fluctuations in characteristic fluid flow parameters like the flow velocity or pressure. Another FIV set focuses on instability-induced excitation which is linked to instabilities within the flow such as vortex shedding or impinging shear layers.

Much research has been conducted for flows over cavities to study the impinging shear flow. However, to our best knowledge, the study of FIV created by impinging flow was rarely considered. Some used the lid-driven cavity model for FIV studies. In this case, the bottom side of the cavity had a deformable plate. However, this setup was not easily modelled in experimental studies since the boundary condition imposed by the lid-driven flow is difficult to replicate in the physical experiment. To avoid such limitations, the author's group designed a channel driven cavity flow (CDCF) setup to study the FIV with a deformable plate at the bottom of the cavity section (Kwon and Arceneaux 2017; Kwon and Bowling 2018).

The objective of the present study was to examine the FIV of the CDCF while the inlet flow was undulated. The study was conducted through a series of physical experiments using a test setup designed and fabricated for the study, which is described later. The undulated flow was generated by controlling a set of solenoid valves. A digital flow meter measured the undulated flow velocity, and a set of laser displacement

✉ Y. W. Kwon
ywkwon2004@yahoo.com

1 Department of Mechanical and Aerospace Engineering, Naval Postgraduate School, Monterey, CA 93943, USA

2 Fakultät Maschinenbau, Helmut-Schmidt-Universität/Universität der Bundeswehr, Hamburg, Germany

3 Department of Aerospace Engineering, United States Naval Academy, Annapolis, MD 21402, USA

sensors recorded the vibrational motion of the plate. Both aluminum alloy and carbon fiber composite plates were tested in the CDCF setup. It is hoped that this study will provide a better understanding of the structural motion as a function of the undulated flow characteristics.

The subsequent section describes the overall experimental setup, and the following section provides description of how undulated flows were generated using a series of solenoid valves. Then, experimental results are presented with discussion. Finally, conclusions are given.

2 Experimental setup

This section describes the design and build process of the experimental setup for the CDCF as well as the overall experimental setup. Additionally, the design, manufacture, and assembly process of the required additional parts are explained. It also presents details regarding how the fluid flow is controlled, what materials have been tested, and what measurement instruments have been used.

A study of FSI is conducted using the experimental setup called CDCF (Kwon and Arceneaux 2017; Kwon and Bowling 2018). This is a modification of a standard lid-driven cavity flow, which is difficult to test experimentally. The CDCF system is shown in Fig. 1. The system consists of a cavity that is connected to a channel at the inlet and outlet section, respectively. Figure 1b shows the actual inner dimensions of the CDCF system. For visual clarity, Fig. 1a shows the system inverted. To ensure the inlet flow is fully developed prior to reaching the cavity section, the inlet channel is long and has a narrow cross-sectional area. The same approach is applied to the outlet channel to enable the outgoing flow to be fully developed before leaving the outlet of the channel. Both the inlet and outlet channels are 101.6 mm wide and 10.16 mm high. The channel sections have such narrow cross-sections that the flow in the channel section remains laminar. The cavity section is 30.48 mm high, and the base is a square of 101.6 mm on each side.

This CDCF system shares geometric similitude to that used in Ref. (Kwon and Arceneaux 2017; Kwon and Bowling 2018) except that the present CDCF system was reduced in size so as to lower the Reynolds number of the flow in the system. The lower Reynolds number minimized turbulence in the flow.

The overall experimental setup consists of a water reservoir, a pump, the channel with cavity and transition parts, solenoid valves with a controlling application, digital flow meters, a clamping apparatus, and measurement equipment. The pump draws water for the system from the water reservoir and provides the channel with a constant mass flow. At the same time, the reservoir serves as a collecting basin for the water that flows from the channel outlet which makes this a closed system. To investigate fluid–structure interaction, the bottom side of the cavity has a flexible plate. A picture of the overall experimental setup is shown in Fig. 2.

To ensure proper flow throughout the entire system and especially in the area between the pipe and the channel, it is

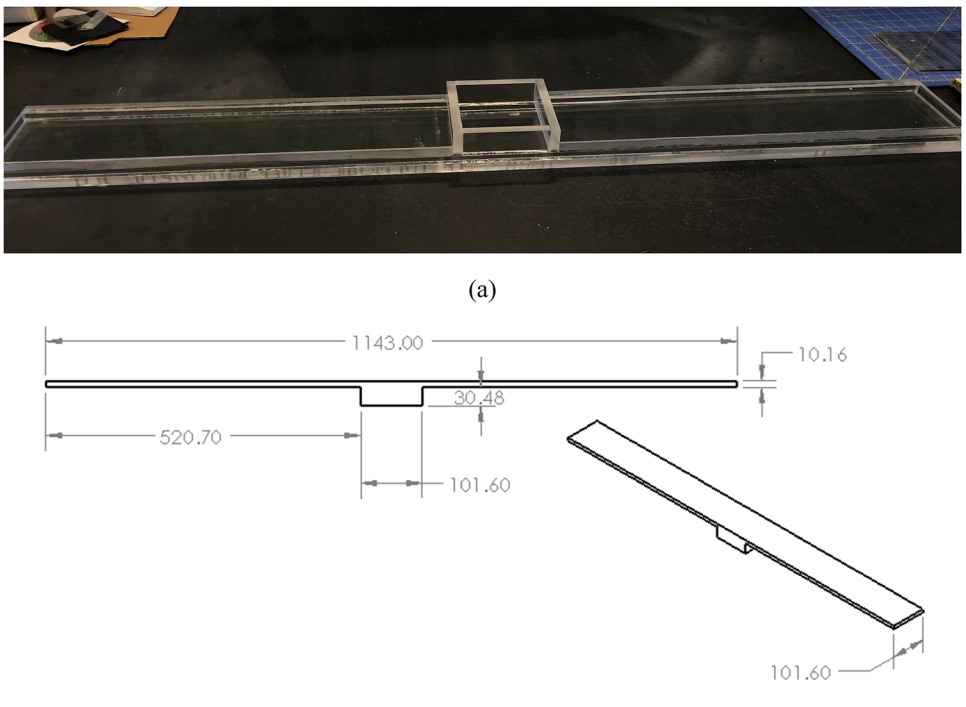

Fig. 1 Channel drive cavity flow (CDCF) system: **a** assembled using Plexiglas and **b** internal dimensions of the system in mm

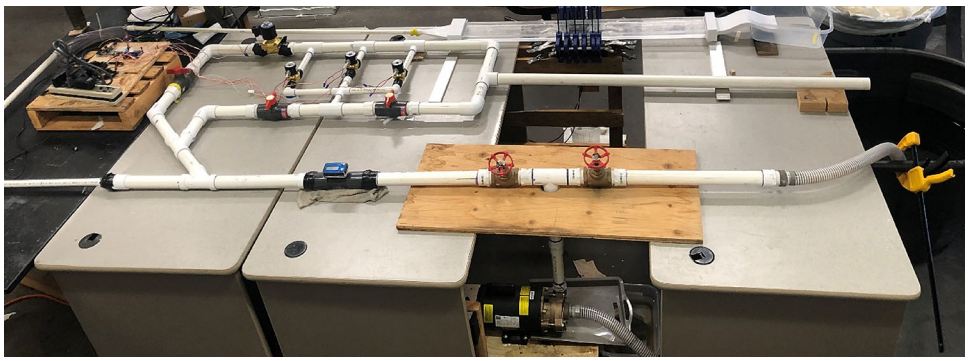

Fig. 2 Test setup

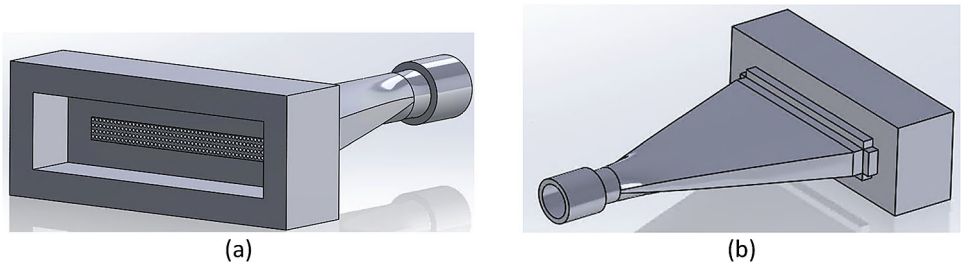

Fig. 3 Different views of the transition piece

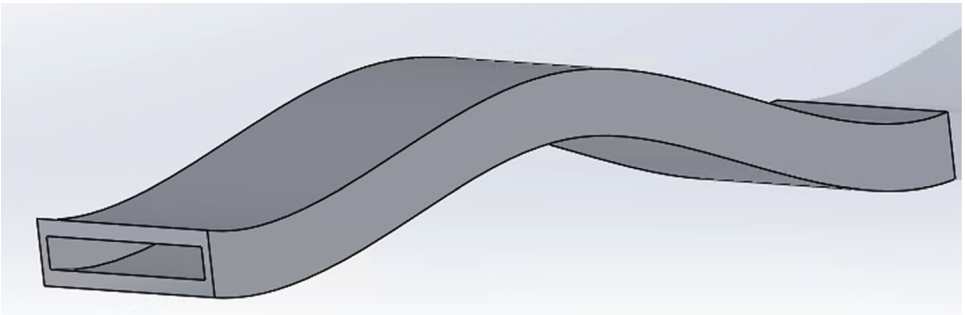

Fig. 4 Outlet transition part

necessary to incorporate a specifically designed transition at the flow channel inlet. The requirements for this part are that it must have a round cross-section on the inlet and transition to a rectangular cross-section at the outlet. So as to ensure a tight fit of the transition section on both sides, this part is designed with slip joints that are press-fitted onto the channel and the pipe. In addition to that, a so-called "flow straightener" is installed. This insert helps reduce swirls and lateral velocity components and thus lowers the degree of turbulence. The result is a nearly uniform, parallel fluid flow. Two different views of the geometry of the transition part are shown in Fig. 3. Figure 3a provides detail regarding the outlet to the flow channel, with embedded flow straightener visible, while Fig. 3b illustrates the inlet.

Furthermore, a transition piece between the flow channel outlet and the water reservoir was designed and manufactured as shown in Fig. 4. This part guarantees that the entire channel is filled with water even when water is not circulated in the system. This was achieved by the transition part having a curved shape with a lower position in the vertex (A) inside the transition piece being higher than the upper edge (B) of the channel as is sketched in Fig. 5.

All parts were manufactured using a 3D printer. Additive manufacturing (i.e., 3D printing) processes use a variety of materials. In this case, polycarbonate was the material utilized since it is a strong thermoplastic. Because the pump provides a constant flow rate, the flow is regulated using a series of solenoid valves which results in an undulating flow to the cavity section. The overall pipe system, which is sketched in Fig. 6, was assembled from PVC (Polyvinyl chloride) Schedule 40 pipe of three different diameters, 12.70 mm, 19.05 mm, and 38.10 mm. All pipes were joined using either threaded connections or PVC solvent welding.

The pipe and valve arrangement allows either a constant or undulated flow. When the manually operated gate valves V1 and V2, as depicted in Fig. 6, are closed, the water only flows on the outer circulation path. The flow can be regulated with the solenoid valves S1–S4 when the valves V1 and V2 are open. It should be noted that solenoid valves S1–S3 are of the type NC (normally closed), while S4 is NO (normally open).

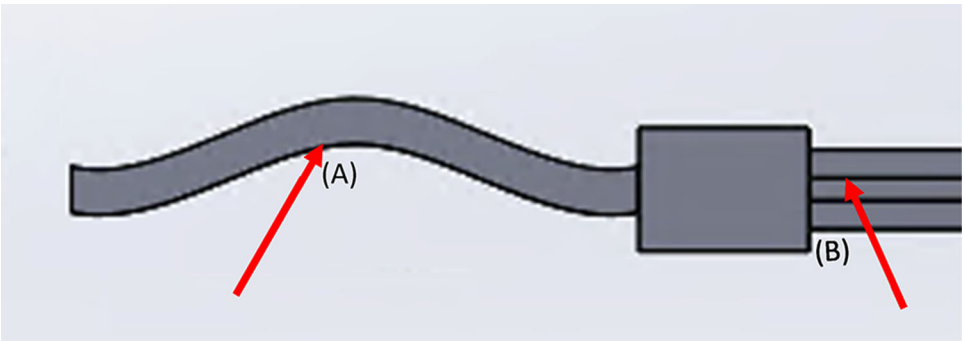

Fig. 5 Assembled outlet transition to the outlet channel

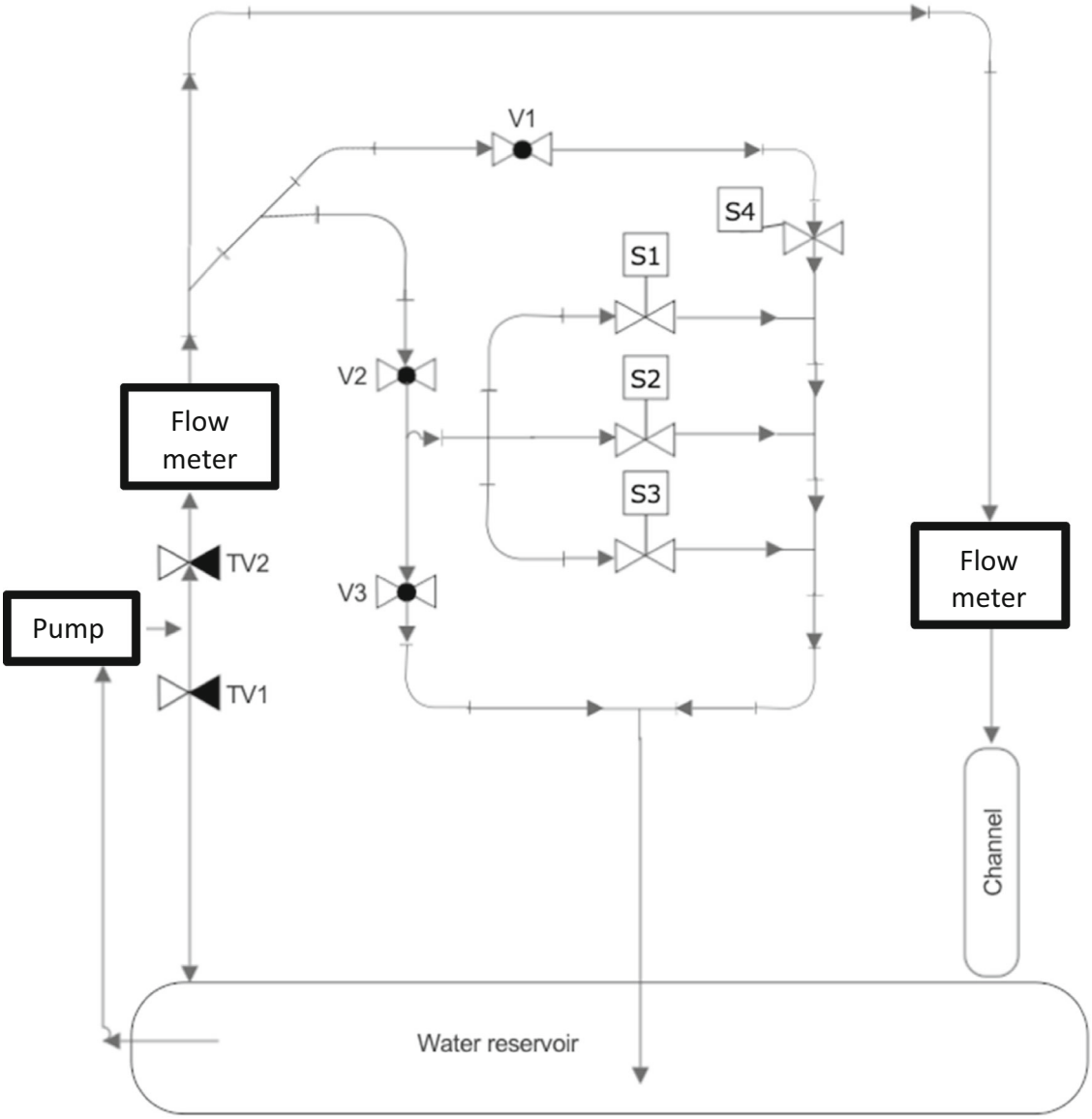

Fig. 6 Schematic of flow diagram using solenoid valves

The throttling valves, TV1 and TV2, and the combination of opening/closing these valves, partially determines the overall flow that is supplied to the system. When TV2 is closed, all of the water drawn by the pump will flow back into the water reservoir if TV1 is open. Likewise, the opposite configuration holds true such that when TV2 is fully open and

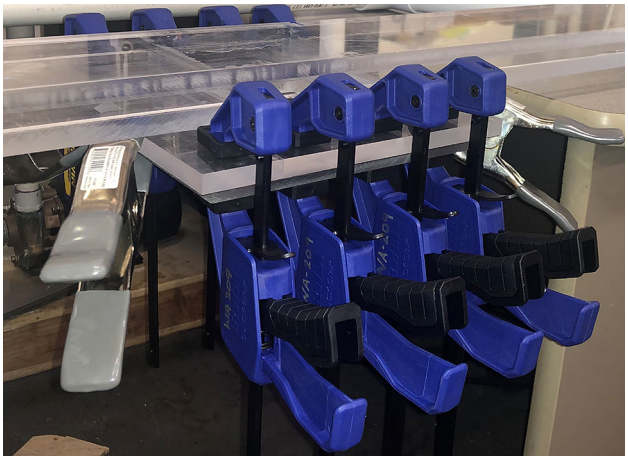

Fig. 7 Test plate clamped at the bottom of the cavity section

TV1 is completely closed, all the water drawn by the pump is provided to the piping system feeding the flow channel.

A flat test plate was attached to the open bottom side of the cavity section using multiple bar clamps as shown in Fig. 7. This was done to represent the clamped boundary condition on the test plate as closely as possible. The plate was 228.6 mm by 228.6 mm and was larger than the opening at the bottom of the cavity section which was 101.6 mm by 101.6 mm. The test plate consisted of either an aluminum alloy or a carbon fiber composite. The aluminum alloy has the density 2700 kg/m^3, elastic modulus 68.9 GPa, Poisson's ratio 0.33, and a thickness of 0.508 mm. The carbon fiber composite was purchased from Dragon Plate©, and the material properties were measured using the testing machine in our lab. It had a unidirectional layup with a density 1350 kg/m^3, longitudinal elastic modulus 117 GPa, transverse elastic modulus 7.14 GPa, and thickness of 0.508 mm.

Laser displacement sensors were used to measure the displacement of the flexible plate at specific locations. The sensor unit consists of two components, a sensor head, and an amplifier unit. The emitted laser has a wavelength of 655 nm (visible red light), an output of 220 μW and is classified as a class 1 laser product according to IEC60825-1. This laser class means that the laser is considered safe for use with the only safety measure being a cautionary warning not to look directly into the laser when energized. The amplifier unit receives the data from the laser and communicates with the National Instrument module NI 9215 and the National Instrument software DAQExpress that logs the received data.

Since the software only logs the output voltage, it needs to be converted into a displacement. The voltage scaling has a range of 10 V, while the sensor head has a measurement range of 25 mm (from 20 to 45 mm). The conversion yields 2.5 μm/mV. This means, a change of 1 mV in the output voltage received from the amplifier unit yields a displacement of 2.5 μm.

To perform an appropriate measurement, the laser needs to be fixed perpendicular to the specific position on the flexible plate. Additionally, the sensor head has to be mounted 30 mm underneath the plate. A wooden pallet and an additional wooden block are used to attach the laser displacement sensors in the correct position. The wooden block was screwed to the pallet and the supplied mounting for the sensor which was attached to this block.

Before starting the experiment, the plate to be examined was clamped to the bottom of the cavity to create the fixed support of the plate edges. A clamping apparatus was used to clamp the plate. It consists of pieces of acrylic that are glued to the outer edges of the cavity to create a square surface. A second square acrylic frame was built to complete the clamping apparatus. The plate was then fixed in between these two surfaces as described previously using racketing bar clamps capable of exerting approximately 950 kPa of camping force.

After successfully clamping the plate, which is now the flexible bottom of the cavity, the cavity and the channel were filled with water to measure the static deflection of the plate. From that point, the water flow velocity was gradually increased, and the displacements were measured for constant flow rates.

Next, the flow condition was changed from a constant flow to an undulated flow. To apply an undulated flow, the valves to the bypass/subsystem were opened. That allowed the quick-acting solenoid valves to work. From here on, different closing and opening times for the valves, which determine the flow frequency, were applied via an Arduino controller.

3 Control of solenoid valve for undulating flow

In the control loop of the flow system, three of the solenoids are attached to three quarter inch piping, and a larger fourth valve is fitted to one- and one-half inch piping. It was found that the desired sinusoidal nature of the undulation was best achieved using the solenoids only on the smaller piping loop. The activation of the larger fourth solenoid increased the flow by a disproportionate amount in relation to the other solenoids, causing an uneven spike in pressure. As a result, during every test, valve V1 in Fig. 6 was partially open, valve V2 is completely open, and valve V3 is always open. In addition, solenoid valve S4 remained open. To achieve the desired sinusoidal shape, the three smaller solenoid valves were cycled as sketched in Fig. 8, which shows when each valve was opened and closed as well as the time duration that each was on. The horizontal axis denotes a time increment which is determined based on the frequency of the undulating flow. Such operation of the valves as shown in Fig. 8 yielded a half pseudo-sinusoidal shape of flow rate with the

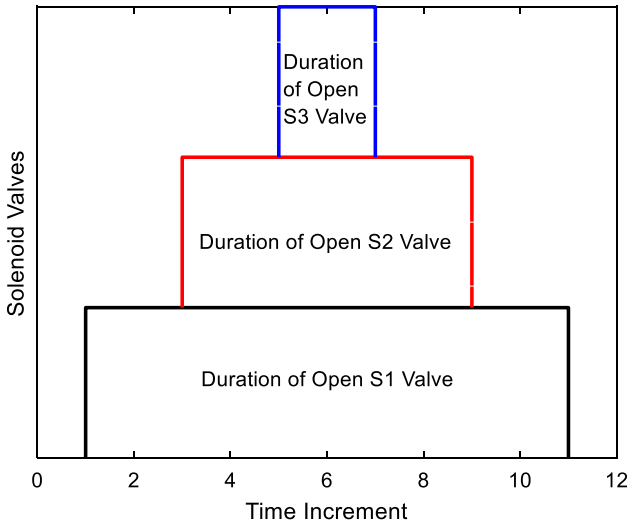

Fig. 8 Opening and closure timing of three solenoid valves

period of 24 Δt, where Δt is the time increment in the figure. The opening and closure of each solenoid valve is not instant. Instead, there is a short delay in opening or closing completely caused by the physical movement of the valve seat. Such a delay makes the flow rate a pseudo-sinusoidal shape with a continuous change as measured using the digital flow meter.

The solenoids were controlled by an Arduino attached to a breadboard. Programming was done in the Arduino Software Integrated Development Environment. The programming behind the solenoid control consisted of two parts. First, the connection port was opened, and all solenoids were deactivated. In the deactivated (powered down) state, the S1–S3 solenoid gate valves are closed. Second, an infinite loop was run to open and close the solenoids per the basic pattern outlined in Fig. 8.

A typical undulating flow measured using the flowmeter located just before the channel section in Fig. 6 is shown in Fig. 9. The raw signal data of the flowmeter contained considerable noise. To remove this, the data were passed through a lowpass Butterworth filter. All high frequency noise was filtered beyond a cutoff frequency of 10 Hz. After filtering, a fast Fourier transformation was used to attain the fundamental frequency of the wave.

Eventually, by selecting proper time increments for the control of the solenoid valves, pseudo-sinusoidal undulating flows with the frequency of 0.5 Hz, 0.75 Hz, 1.0 Hz, 1.25 Hz or 1.5 Hz could be obtained and were used in the FSI study.

4 Experimental results

Experiments were conducted for different undulation frequencies as well as different flow rates. The frequencies were varied from 0.5 to 1.25 Hz with a 0.25 Hz increment. The mean flow speed in the inlet channel was changed incrementally. While the frequency was controlled using the solenoid valves, the flow rate was controlled using the TV1 and TV2 valves. The TV1 valve was fully open for all the tests while TV2 valve was used for achieving different flow rates. Table 1 shows the mean flow speed in the inlet channel and the velocity amplitude resulting from the controlled solenoid valves at the undulation frequency of 1.0 Hz. The maximum velocity is the sum of mean velocity and the velocity amplitude while the minimum velocity is the velocity amplitude subtracted from the mean velocity. The flow velocity decreased very slightly as the undulation frequency increased from 0.5 to 1.25 Hz. However, the change was quite small.

4.1 Aluminum plate

Before conducting the test, the natural frequency of the aluminum plate was determined. This was done to determine whether the flow excitation frequency would be close enough to the natural frequency to possibly result in creating resonance. While the boundary condition of the plate during the test was intended to represent the clamped boundary condition along all edges, the actual condition might not be fully clamped. Instead, the actual boundary condition is believed to be between the clamped and simply supported cases while being closer to the clamped boundary condition. As a result, the first three natural frequencies of both clamped and simply supported boundary conditions were computed as listed in Table 2 from the eigenvalue analysis of the plates using the finite element method. Even though the added mass effect was considered to reduce the natural frequency because of the fluid–structure interaction, the natural frequency was still much greater than the flow excitation frequency. Therefore, there was no possibility of vibrational resonance of the plate.

Two displacement sensors were located as sketched in Fig. 10. One is located at the center of the plate while the other is near the inlet side. The length from the inlet side to the outlet side along the plate was divided equally by four, and the inlet side sensor is located at the center between the inlet and the center of the plate.

All the displacement measurements were referenced to the initial state with zero deflection of the plate without water in the CDCF section. Therefore, the measured deflections included both hydrostatic displacement resulting from the water in the cavity section and the displacement due to the undulated flows. When the plate deflected downward, i.e., bulging outside of the cavity, it was considered positive. This convention is used in all subsequent plots unless mentioned otherwise.

During the experimental testing, the flow rate and undulation frequency were systematically varied. Each data set was measured for at least ten seconds, and the measurement

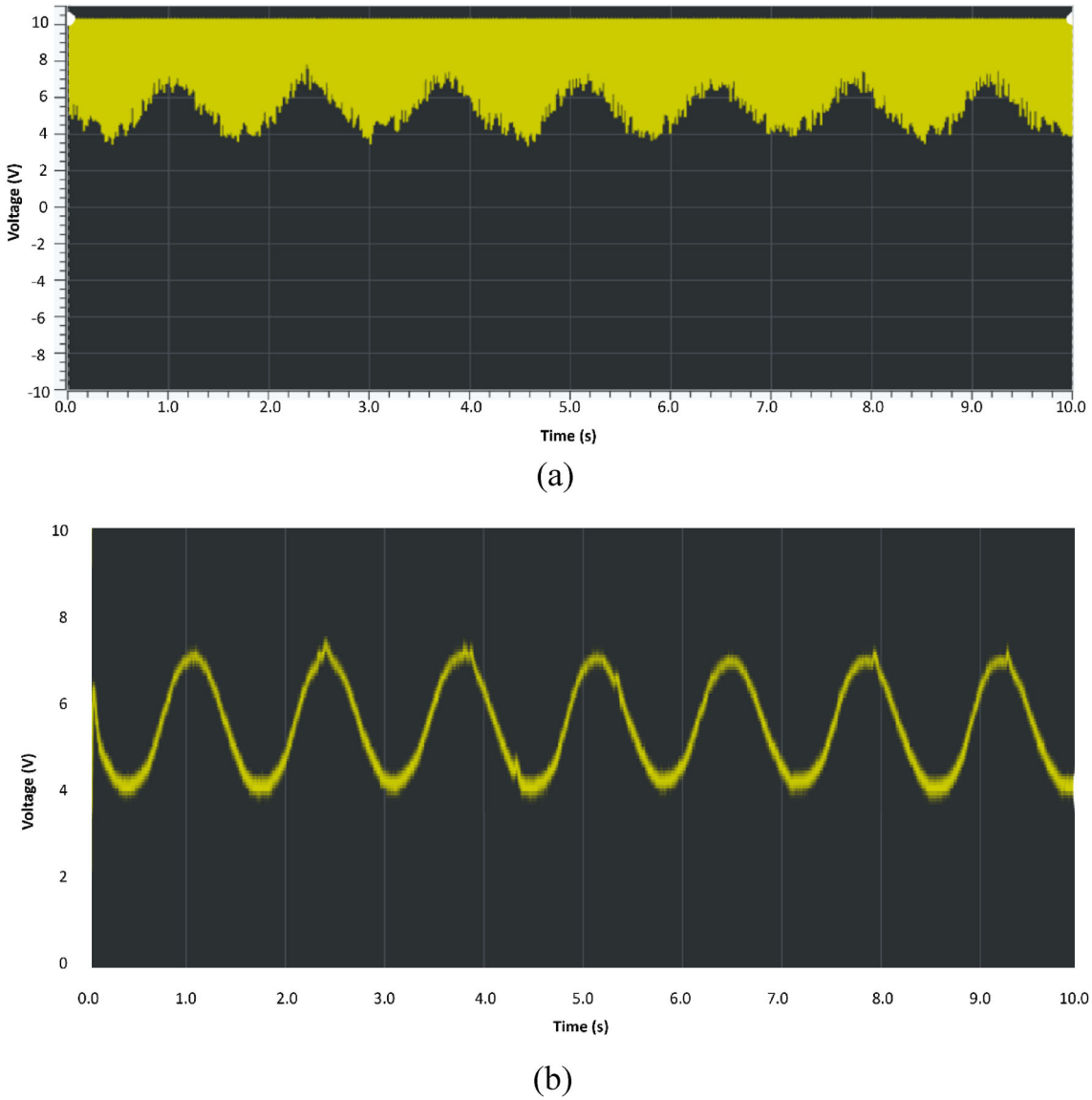

Fig. 9 Flow rate measured using a digital flowmeter. **a** Raw data and **b** filtered data

Table 1 Tested undulated flow velocities at 1 Hz

Mean. velocity (m/s)	Amp. of velocity (m/s)
0.0727	0.0724
0.109	0.104
0.145	0.135
0.182	0.167
0.218	0.198
0.254	0.230
0.291	0.261

Table 2 Natural frequencies of dry aluminum plate with 0.508 mm thickness

Mode	Clamped BC (Hz)	Simply supported BC (Hz)
1	2738	1051
2	5584	4221
3	8238	6595

was repeated at least three times to confirm the repeatability of the test results. The measured deflections of the plate showed periodic motions. Even though the undulated flows had sinusoidal flow rates, the vibrational characteristics of the plate were much more complex than the sinusoidal shapes, including high frequency modes, an occurrence which was discussed in the previous experimental and numerical studies of fluid–structure interaction (Kwon and Plessas 2014;

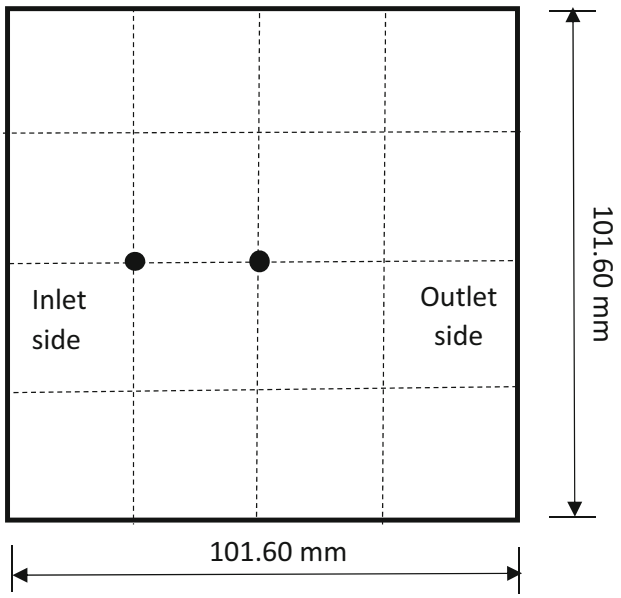

Fig. 10 Location of measured displacement of the plate in CDCF

Kwon et al 2013; Kwon 2020). The dominant vibrational frequencies of the plate included the undulating frequency of the flow in addition to other frequencies. However, the peak deflections and maximum flow rates did not occur at the same time. That is, there is a difference in phase between the flow oscillation and plate vibration.

Figure 11 shows the deflections at the center of the aluminum plate for different undulated frequencies of the flow at the average velocity of 0.180 m/s at the inlet channel. As the flow frequency changed from 0.5 to 0.75 Hz, the magnitude of the deflection of the aluminum plate increased very noticeably. However, any further increase in the flow frequency had a smaller effect on the magnitude of the deflection. In addition, the maximum and minimum deflections during one cycle period occurred one after the other for the 1.0 Hz and 1.25 Hz flows while those were more separated in time for the 0.5 Hz and 0.75 Hz. The mean vibrational amplitude of the plate during each cycle varied slightly with the undulation frequency of the flow. This was found to be the greatest for the 0.5 Hz flow and least for the 1.0 Hz flow.

The frequency spectra of the deflection time-history of the aluminum plate from Fig. 11 were obtained using the fast Fourier transform technique, which is shown in Fig. 12. As visually observed in the time-history plots, the frequency spectra indicated that the vibration of the plate contained not only the frequency of the undulated flow but also other frequencies. For all different undulated flows, the vibrational frequencies of the aluminum plate were mostly confined between the undulated flow frequency and 5.0 Hz. The noticeable peaks in the frequency domain occurred at or very close to the multiples of the flow frequency until around 5.0 Hz. Among them, there were three or four much more dominant peaks that contributed to the major parts of the vibrational motion of the plate. One of them was the undu-

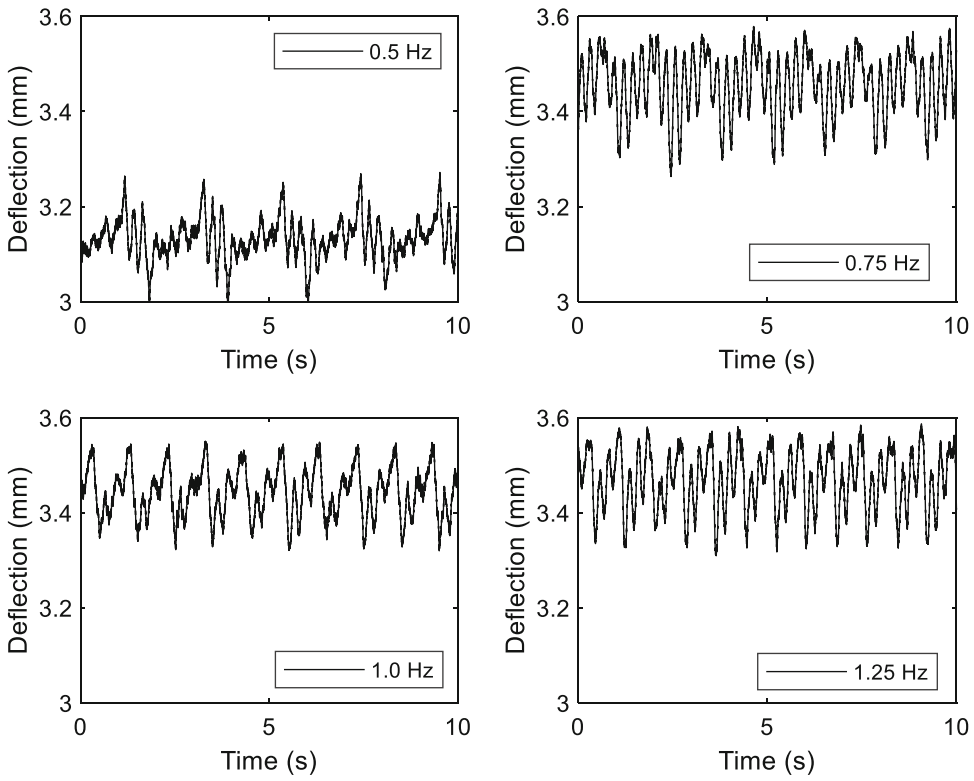

Fig. 11 Deflection of the aluminum plate for different frequencies of undulated flow at the average inlet channel velocity of 0.180 m/s

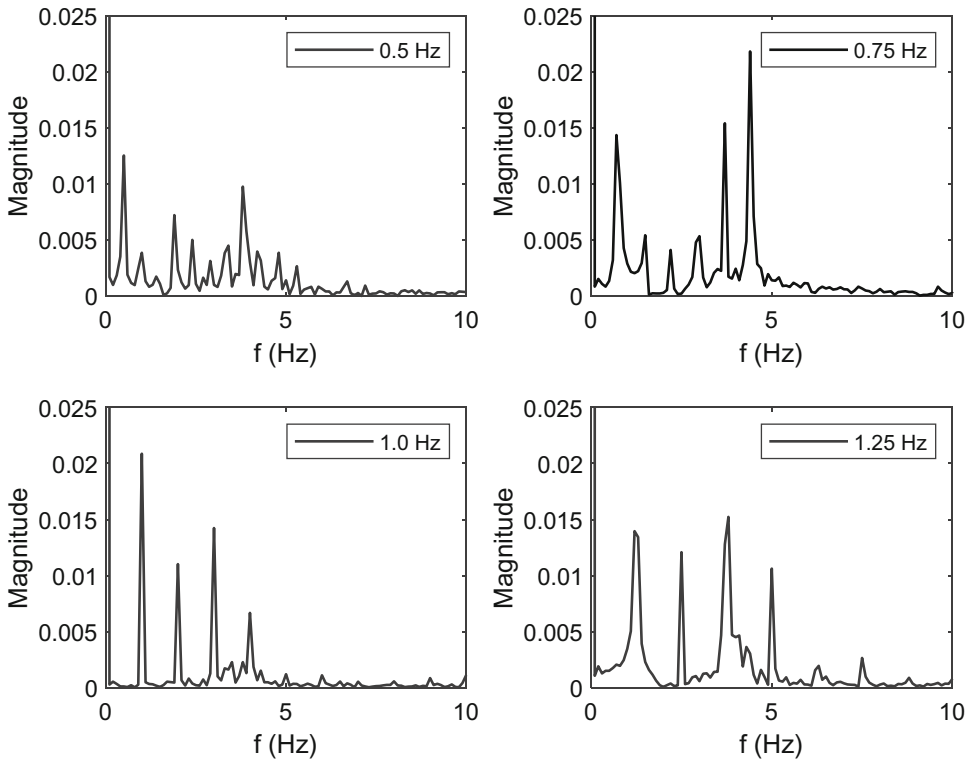

Fig. 12 Frequency spectra of the time-history of Fig. 11

lated flow frequency, as expected. For the flow frequencies of 0.5 Hz and 1.0 Hz, the largest magnitude of the plate frequencies occurred at the flow frequency. However, for other flows with 0.75 Hz and 1.25 Hz, the greatest magnitude of the plate frequencies occurred at higher frequencies than the flow frequency. This was more obvious for the 0.75 Hz flow with the largest magnitude at 4.4 Hz. The flow with 0.5 Hz showed less pronounced peaks but more peaks in the frequency spectrum. This suggests that the plate vibration has a sizable contribution from more diverse frequencies. This possibly indicates that the added mass effect for the flow with 0.5 Hz is more complicated than in other cases. For further understanding, flow visualization and/or further numerical analysis are necessary. This will be conducted in future study.

Figure 13 compares the deflections at the center and the inlet locations for the undulated flow of 1.0 Hz with the average inlet channel speed 0.145 m/s. The center location had a greater deflection as well as larger vibrational amplitude as expected, but the vibrational characteristics were nearly identical between the two locations.

The effect of varying the flow rates under the same flow frequency was studied as shown in Figs. 14 and 15. The former is for 0.5 Hz while the latter is for 1.0 Hz. Figure 15 indicates that the magnitude of oscillatory vibration of the plate becomes larger as the flow velocity increases at the frequency of 1 Hz. Figure 14 also shows a similar trend at 0.5 Hz, but the magnitude of vibration was similar between the average inlet channel speed 0.218 m/s and 0.291 m/s at 0.5 Hz.

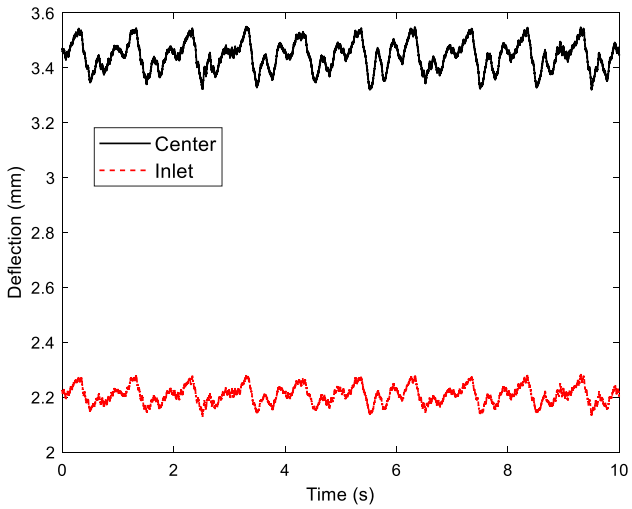

Fig. 13 Deflection of the aluminum plate at center and inlet locations for 1.0 Hz flow with the velocity 0.145 m/s

Figure 16 plots the vibrational magnitude, which was determined the difference between the representative maximum and minimum deflections, as a function of the flow velocity at 0.5 Hz and 1.0 Hz of flow frequency, respectively. The plot shows two different behaviors. The vibrational magnitude with 1.0 Hz was approximately a linear function of the flow velocity for all tested flow velocities. However, the vibrational magnitude with 0.5 Hz was more or less linear until

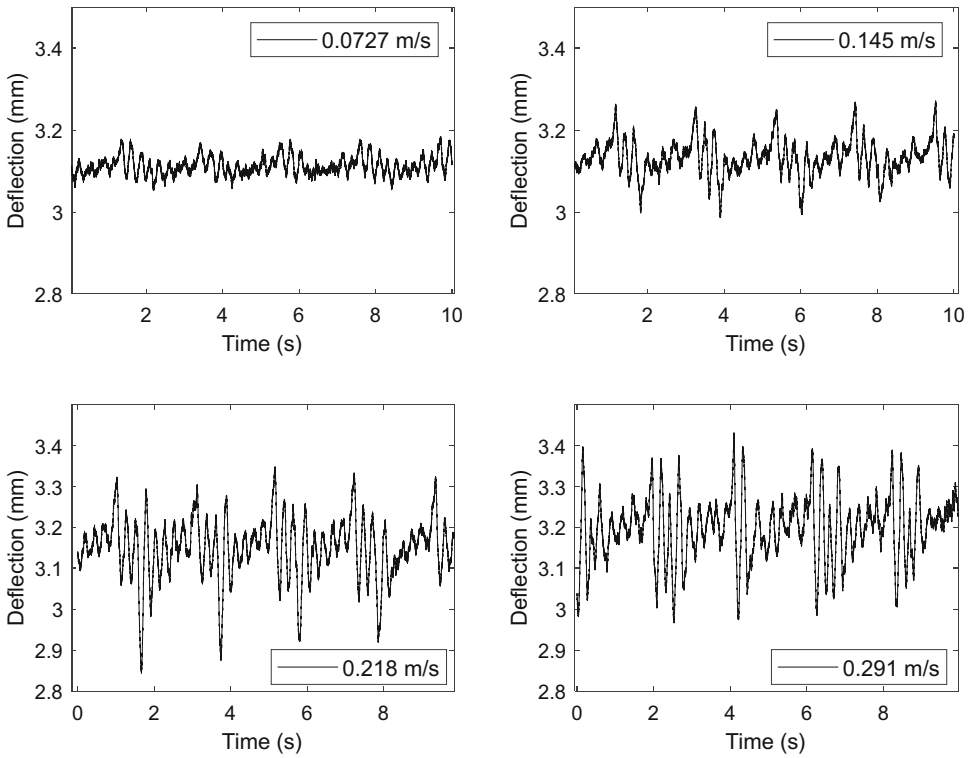

Fig. 14 Deflection of the aluminum plate for different average flow velocities of undulation frequency 0.5 Hz

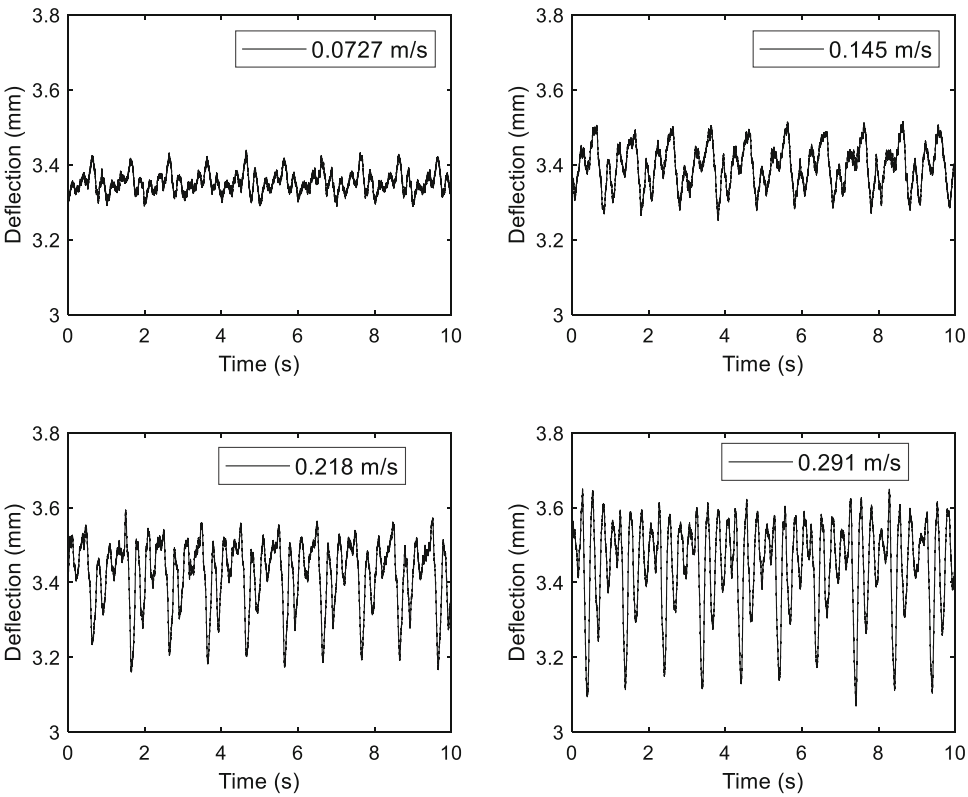

Fig. 15 Deflection of the aluminum plate for different average flow velocities of undulation frequency 1.0 Hz

0.218 m/s where it begins to show a kind of plateau deviating from the increasing flow velocity.

When Figs. 14 and 15 were compared for the same flow rates but at different flow frequencies, the vibrational pattern becomes more different between the two different flow frequencies as the flow rate increases. In other words, when the flow rate is 0.291 m/s, the vibrational shape looks very different between 0.5 and 1.0 Hz. It is also observed that the

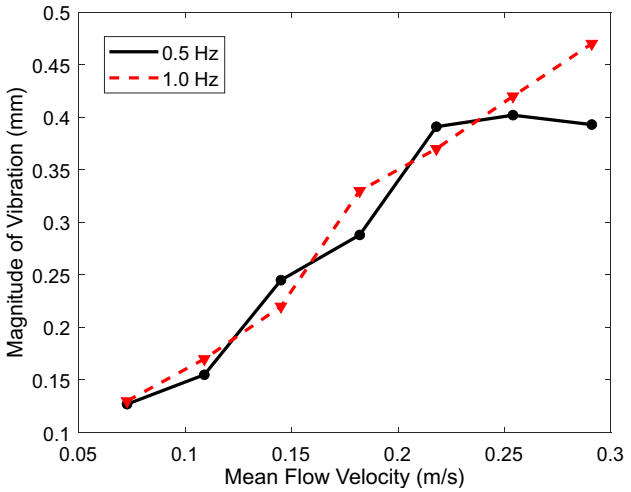

Fig. 16 Magnitude of vibration of the aluminum plate as a function of flow velocity

maximum and minimum deflections of the aluminum plate within each period of flow oscillation showed a balanced behavior for the slow flow velocities such as 0.0727 m/s and 0.145 m/s regardless of the flow frequency. However, the minimum deflection was more protruded for the average flow velocity 0.218 m/s and 0.291 m/s at 1.0 Hz.

Figure 17 plots the frequency spectra of the time-history of the aluminum plate vibration as shown in Fig. 14 with 0.5 Hz. The frequency plot shows that the major peaks in the frequency domain generally increase their magnitudes with the increasing flow speed. When the flow speed was 0.291 m/s, there were several major frequencies that had larger magnitudes than the flow frequency 0.5 Hz.

5 Composite plate

The next set of experiments conducted was for a unidirectional carbon fiber composite. Since the composite plate has different stiffnesses depending on its orientation, two different orientations were tested. Figure 18 shows the two different fiber orientations relative to the flow direction. When the fibers lie along the direction of flow, it is called the 'fiber orientation' of the composite plate. On the other hand, if the fibers are in the perpendicular direction to the flow, it is called the 'matrix orientation' of the composite plate.

Since the unidirectional fibrous composite has a much greater stiffness along the fiber direction than the matrix direction, the composite plate in the matrix orientation had larger deflections than the plate tested in the fiber orientation. This is evident through the comparison of the deflections presented in Figs. 19 and 20. All the tests using composite plates were conducted at the undulation frequency of 1.0 Hz while the flow velocity was varied.

Like the aluminum plate, the amplitude of vibration increased with the flow velocity regardless of the orienta-

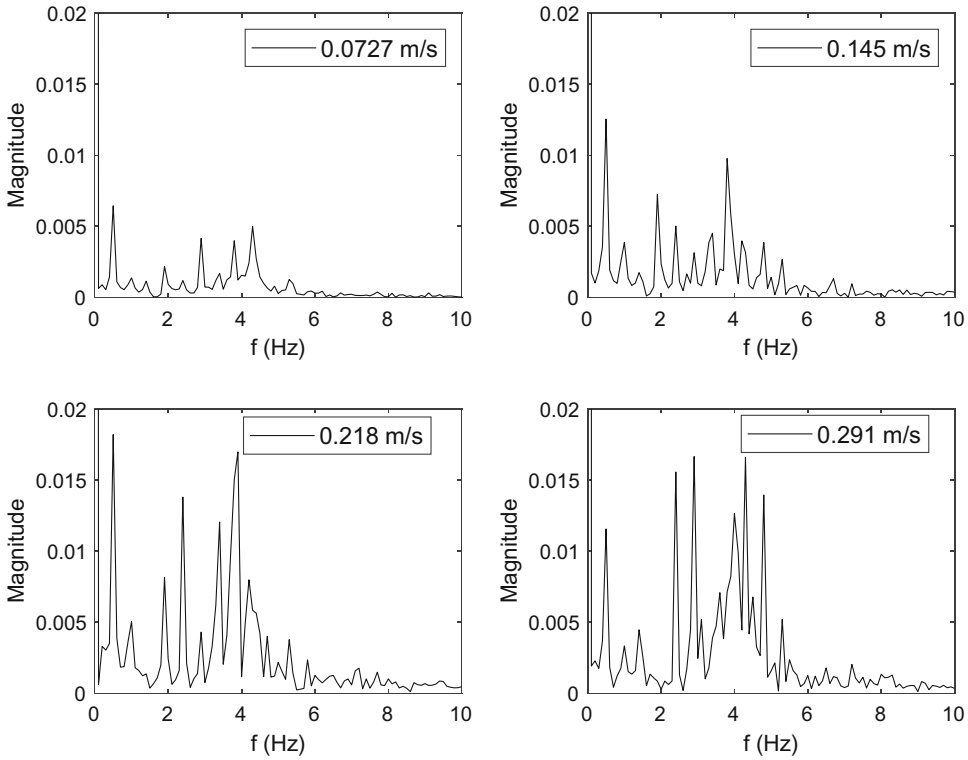

Fig. 17 Frequency spectra of the time-history of Fig. 14 at 0.5 Hz

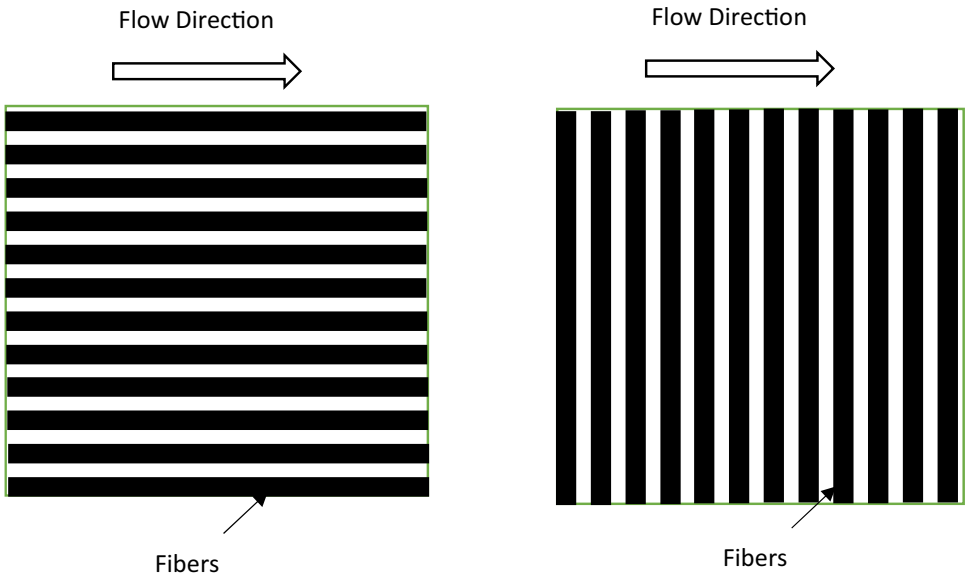

Fig. 18 Two different orientations of fibrous composite plate: (left) fiber orientation, (right) matrix orientation

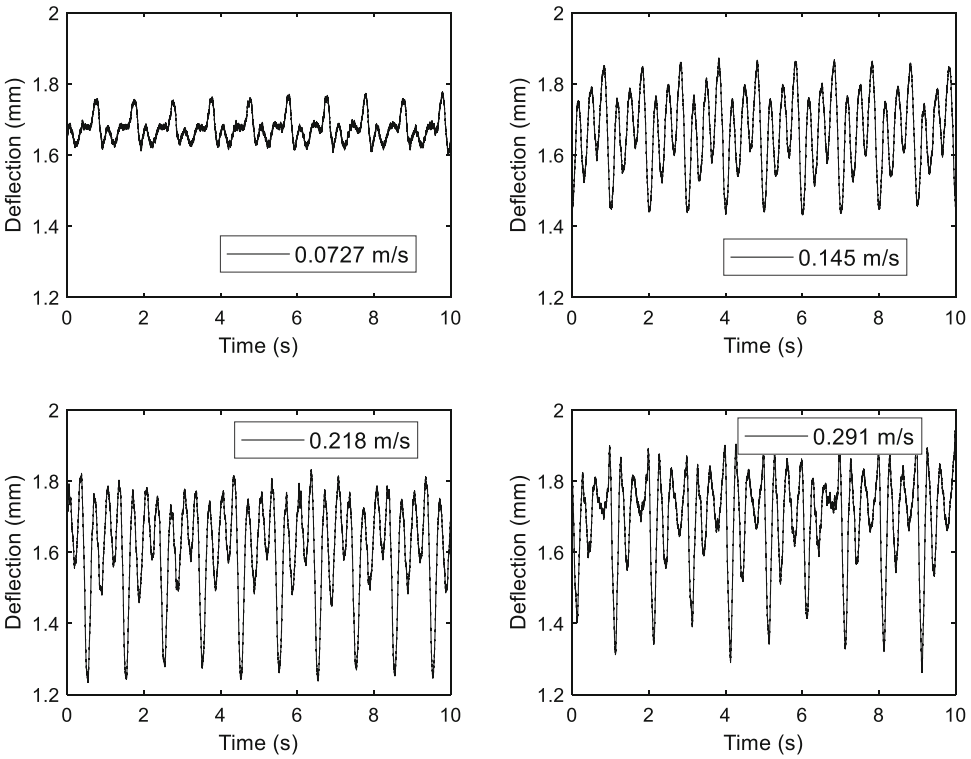

Fig. 19 Center deflection of the unidirectional composite plate at the matrix orientation with various average flow velocities and frequency 1.0 Hz

tion of the composite plate. The vibrational characteristics of the composite plate looked similar between the two different orientations when Figs. 19 and 20 were compared. For better comparison, frequency spectra were obtained for the vibrations as plotted in Figs. 21 and 22.

For the average flow speed 0.0724 m/s, the most dominant frequency of the composite plate was the same as the flow frequency 1.0 Hz, regardless of the plate orientation. For other flow rates, the most dominant frequency of the composite plate was always 3.0 Hz which was more obvious for the composite plate in the matrix orientation. Even though 3.0 Hz is the most dominant frequency of the composite plate, the contribution at 3.0 Hz became relatively smaller for the composite plate of the fiber orientation as compared to that of the matrix orientation. It is not clear why 3.0 Hz was mostly the dominant frequency of the response of the composite plate. It is believed to be related to the stiffness and mass of the plate. However, additional studies are required for clarification.

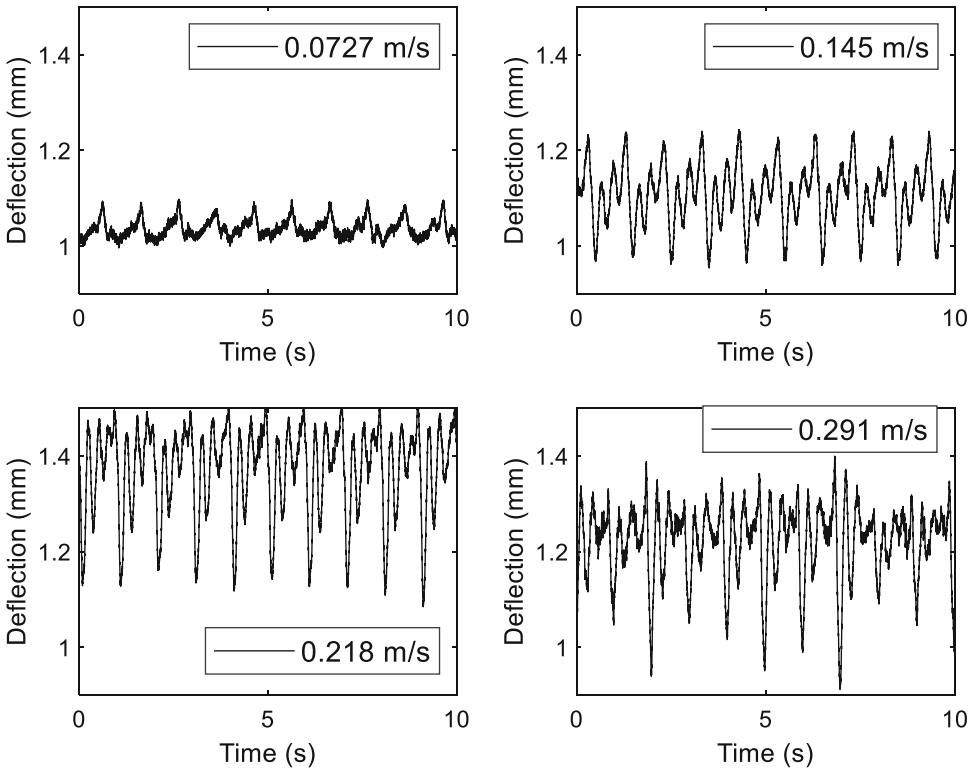

Fig. 20 Center deflection of the unidirectional composite plate at the fiber orientation with various average flow velocities and frequency 1.0 Hz

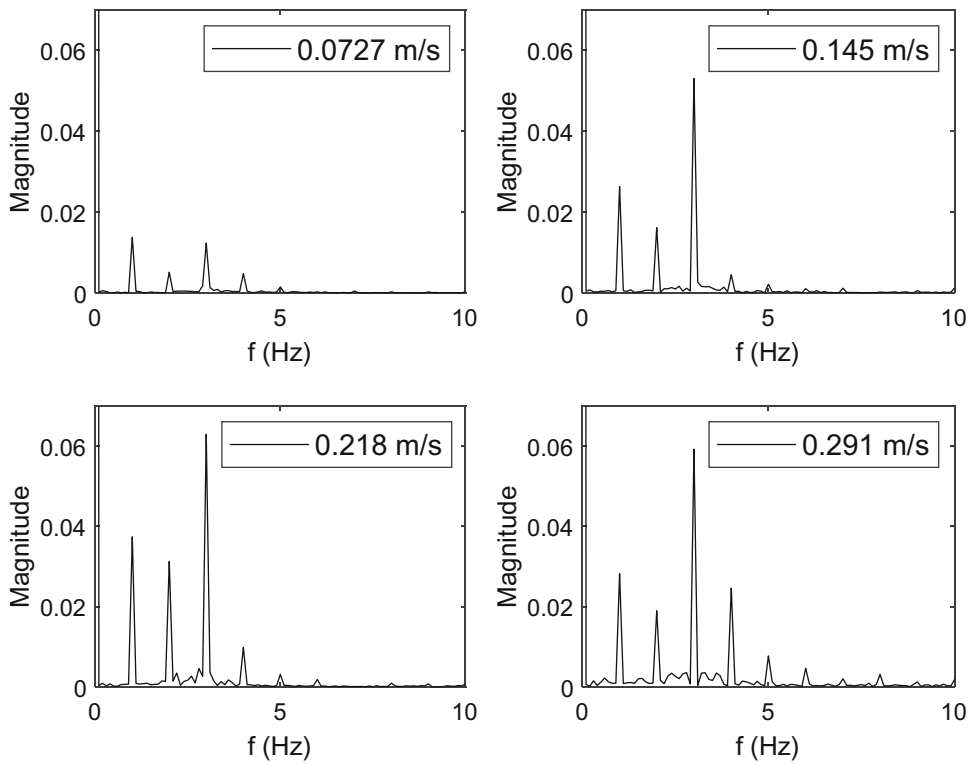

Fig. 21 Frequency spectra of the time-history of Fig. 19

6 Conclusions

The purpose of this study was to investigate fluid–structure interaction with a focus on undulated flow conditions using the CDCF setup. The experimental study was conducted for undulation frequencies in the flow from 0.5 to 1.25 Hz with a 0.25 Hz increment at average inlet flow velocities from

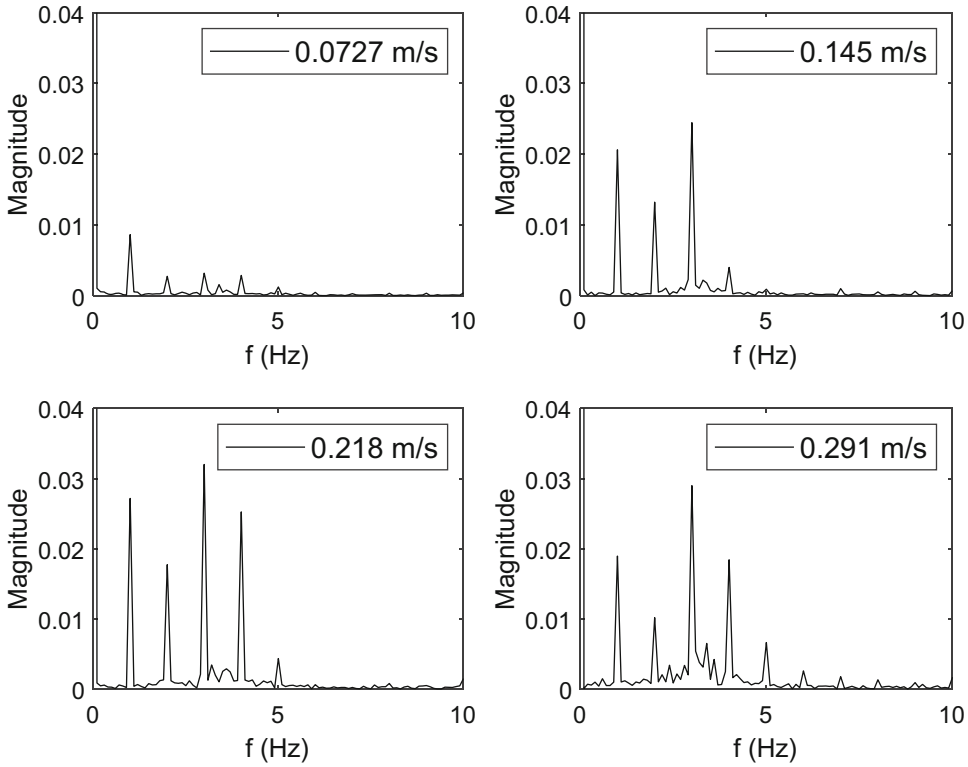

Fig. 22 Frequency spectra of the time-history of Fig. 20

0.0724 to 0.261 m/s. Both aluminum and carbon fiber composite plates were tested.

The undulated flow-induced vibration of the aluminum plate was found to have dominant frequencies occurring from the undulated flow frequency to around 5.0 Hz for the test ranges conducted here. The major peak frequencies were at or very close to the multiples of the undulated frequency. The most dominant vibrational frequency of the aluminum plate was the same as the flow frequency at 0.5 Hz and 1.0 Hz. However, the most dominant frequency occurred at other frequencies for the flow when undulated at 0.75 Hz and 1.25 Hz.

The vibrational amplitude of the aluminum plate increased with the mean flow speed until 0.218 m/s for all the flow frequencies tested in the study. Beyond that flow speed, the change in the vibrational amplitude was different depending on the flow frequency. For example, the plate with 0.5 Hz flow excitation showed a negligible change in the vibrational amplitude beyond the flow speed while the plate with 1.0 Hz excitation had a continuous increase in its vibrational amplitude.

As expected, the vibration of the unidirectional fibrous composite had different deflections depending on the orientation of the plate relative to the flow direction. However, the dominant frequencies of the vibration of the composite plate were very close between the two different plate orientations. Except for 0.5 Hz, all the composite tests indicated that 3.0 Hz was the most dominant frequency regardless of the plate orientation. Its dominance was more severe for the plate of the matrix orientation.

The studies showed that there was a phase difference between the undulated flow and the plate vibration. Such a phase difference became smaller as the flow frequency increased.

Acknowledgements This work was sponsored by the Office of Naval Research. The authors also appreciate the support by Dr. C. Park for his assistance with collecting the test apparatus.

Declarations

Conflict of interest The authors do not have any conflict of interest associated with this research.

Data availability All the data are provided in the paper.

References

Blake WK (2017a) Mechanics of flow-induced sound and vibration, volume 1: general concepts and elementary sources, 2nd edn. Academic Press, New York

Blake WK (2017b) Mechanics of flow-induced sound and vibration, volume 2: complex flow-structure interactions, 2nd edn. Academic Press, New York

Blevins RD (1977) Flow-induced vibration. Van Nostrand Reinhold Co., New York

Blevins RD (1979) Flow-induced vibration in nuclear reactors: a review. Prog Nucl Energy 4(1):25–49

Chen YN (1968) Flow-induced vibration and noise in tube-bank heat exchangers due to von Karman streets. J Eng Ind 90(1):134–146

Kwon YW (2020) Fluid-structure interaction of composite structures. Springer Nature, Switzerland

Kwon YW, Arceneaux SM (2017) "Experimental study of channel driven cavity flow for fluid–structure interaction. J Press Vessel Technol 139:1–5

Kwon YW, Bowling JD (2018) Experimental study of vibration of metallic and composite plates inside channel driven cavity flow. Multisc Multidiscip Model Exp Des 1:211–220

Kwon YW, Plessas SD (2014) Numerical modal analysis of composite structures coupled with water. Compos Struct 116:325–335

Kwon YW, Priest EM, Gordis JH (2013) Investigation of vibrational characteristics of composite beams with fluid-structure interaction. Composite Struct 105:269–278

Leonard A, Roshko A (2001) Aspects of flow-induced vibration. J Fluids Struct 15(3–4):415–425

Nakamura T, Kaneko S, Inada F, Kato M, Ishihara K, Nishihara T, Mureithi N, Langthjem M (2013) Flow-induced vibrations: classifications and lessons from practical experiences, 2nd edn. Academic Press, New York

Naudascher E, Rockwell D (1994) Flow-induced vibrations: an engineering guide. Dover, Illinois

Pettigrew MJ, Taylor CE, Fisher NJ, Yetisir M, Smith BAW (1998) Flow-induced vibration: recent findings and open questions. Nucl Eng Des 185(2–3):249–276